

Transactions, SMiRT-25
Charlotte, NC, USA, August 4-9, 2019
Division V

ALKALI AGGREGATE REACTION IN NUCLEAR CONCRETE STRUCTURES: MODELLING AND LABORATORY TESTS ON A REINFORCED SHEAR WALL

Damien Ghenassia¹, Etienne Grimal¹, Etienne Gallitre²

¹ Civil Engineer, EDF Hydro Engineering Center, Chambéry, FRANCE (damien-externe.ghenassia@edf.fr)

² Civil Engineering expert, EDF Technical Direction, Lyon, FRANCE

ABSTRACT

Some civil engineering structures are affected by concrete pathologies, and degradation mechanisms have been observed. For the management and monitoring of aging hydro and nuclear facilities, laboratory testing and modeling are necessary.

EDF (Electricité de France) has simulated the behaviour of shear walls suffering of an Alkali Aggregate Reaction (AAR) under cycling loading and compared them to experimental results. The RGI model (Réactions de gonflement interne) integrated in Code_Aster has been used and has reproduced successfully the AAR and the loading tests. The simulated peak strength of the wall capacity and the cracking pattern are similar to the experimental results. The peak strength of the AAR wall after 260 days of accelerated aging is higher than for the regular wall despite the degradation of the concrete properties due to AAR. This is explained by the prestress of the concrete due to the swelling of the concrete and the presence of reinforcements. The experimental results for the walls after 610 days and 980 days of accelerated aging show a loss of ductility that the model has not reproduced.

INTRODUCTION

There is a need for reliable simulations of concrete structures with concrete degradation up to the load level leading to their failure. To confirm the reliability of simulations results, the OECD (Organisation for Economic Cooperation and Development) nuclear agency has launched a benchmark called ASCET (Assessment of Structure subject to Concrete Pathologies): 5 reinforced shear walls (1.8m x 1.44 x 0.55m) have been tested at the University of Toronto under vertical static loading and cycling lateral loading. 2 of these walls are built with regular concrete, and the 3 others are built with reactive concrete. EDF has run simulations of the accelerated aging and of the loading tests with the RGI model integrated in Code_Aster. The simulation results are compared with the laboratory results.

CONCRETE MODEL DESCRIPTION

The RGI model has been developed by EDF and the Laboratoire Matériaux et Durabilité des Constructions (LMDC) Toulouse. It is integrated in Code_Aster. The model is able to reproduce concrete pathologies: AAR, also called ASR (Alkali-Silica Reaction), and DEF (Delayed Ettringite Formation). The model is based on elementary physical principles that lead to the formulation of a visco-elasto-plastic orthotropic damage model including chemical pressure induced by the AAR due to a poro-mechanics framework. The anisotropic plasticity and damage allow the realistic modelling of the strong cracking and swelling anisotropy observed on affected structures. It also considers the anisotropic stiffness recovery due to oriented crack reclosing during cyclic loading. A creep model is also integrated. This model is also explained in [5].

Rheological model

The concrete behaviour is modelled in the poro-mechanical framework. The model contains a damage model (inspired from Grimal and al., 2008, [3]), and a rheological model (Sellier and al., 2016, [9]), in order to consider realistic interactions between AAR, creep, shrinkage and damage. In Figure 1, P_g is the pressure induced by AAR and P_w the capillary pressure causing shrinkage in non-saturated conditions.

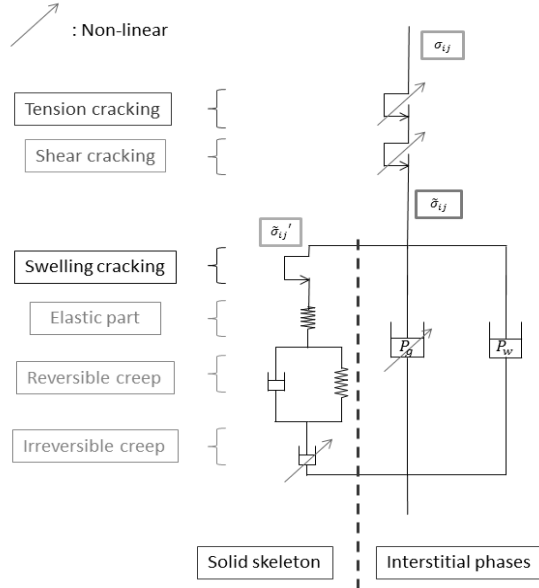


Figure 1 : Rheological scheme of the model

AAR modelling

The gel pressure P_g depends on the AAR advancement A^{aar} which varies according to equation 1 from 0 (before the start of the reaction) to 1 (when the reaction ends). Its evolution principally depends on the temperature and the humidity of the material (equation 1). τ_{ref}^{aar} is a characteristic time which gives a mean representation of the different mechanisms of AAR-gel production (diffusive phenomenon and silica reactivity). It can be obtained by calibration against measured expansion. $A^{aar,\infty}$ is the maximal advancement value reachable according to environmental conditions [4].

$$\frac{\partial A^{aar}}{\partial t} = \frac{1}{\tau_{ref}^{aar}} C^{T,aar} C^{W,aar} (A^{aar,\infty} - A^{aar}) \quad (1)$$

Temperature effect ($C^{T,aar}$) is managed by an Arrhenius' law (equation 2), where E^{aar} is the chemical activation energy ($\approx 40,000$ J/Mol [1]) and T_{ref} the reference temperature for which τ_{ref}^{aar} has been set.

$$C^{T,aar} = \exp\left(-\frac{E^{aar}}{R} \left(\frac{1}{T} - \frac{1}{T_{ref}}\right)\right) \quad (2)$$

When the material is not saturated, reaction kinetics is slowed down. The parameter $C^{W,aar}$ manages this phenomenon (equation 3). S_r represents the saturation degree and $S_r^{th,aar}$ the saturation degree threshold below which the reaction stops.

$$C^{W, aar} = \begin{cases} \left(\frac{S_r - S_r^{th, aar}}{1 - S_r^{th, aar}} \right) & \text{if } S_r > S_r^{th, aar} \\ 0 & \text{if } S_r \leq S_r^{th, aar} \end{cases} \quad (3)$$

The fraction of gel produced by the reaction is ϕ_g . It is the product between the advancement and the maximum gel potential ϕ_g^∞ (equation 4).

$$\phi_g = \phi_g^\infty \cdot A^{aar} \quad (4)$$

AAR mechanical effects

The gel produced applies a pressure P_g (equation 5) on aggregate and concrete (Figure 1). It mainly depends on the accessible porosity (ϕ_v^g), the initial value and the value created by strains (elastic or plastic).

$$p_g = M_g \left(\phi_g - \left(\phi_v^g \left(\frac{P_g}{P_g^{lim}} \right) + b_g \text{Tr}(\varepsilon) + (1 - b_g) \text{Tr}(\varepsilon^{p, g}) \right) \right) \quad (5)$$

$b_g \text{Tr}(\varepsilon)$ is the variation of the porosity due to concrete strain. $\text{Tr}(\varepsilon^{p, g})$ is the variation of the porosity due to plastic AAR-strains. M_g is the gel-matrix modulus. ϕ_v^g is the fraction of gel which does not participate to expansion under the characteristic pressure P_g^{lim} . P_g^{lim} is the pressure necessary to micro-crack the solid skeleton in a specimen free of stresses.

The expression for P_g (5) is managed in two main parts. When $P_g > P_g^{lim}$, the gel spreads in the connected pores under pressure. The second part of the expression represents the pore volume created by strains, which also absorbs part of the gel. The entire volume created by strains (except the AAR plastic volume) is affected by the Biot coefficient b_g which comes from poromechanical considerations [7,1]. Grimal's model gives the calibration of b_g lying between 0.1 and 0.4. For plastic strains induced by the AAR ($\varepsilon^{p, g}$), $b_g = 1$ because cracks created by the gel are considered to be always accessible for the gel and therefore totally filled by it (Figure 2).

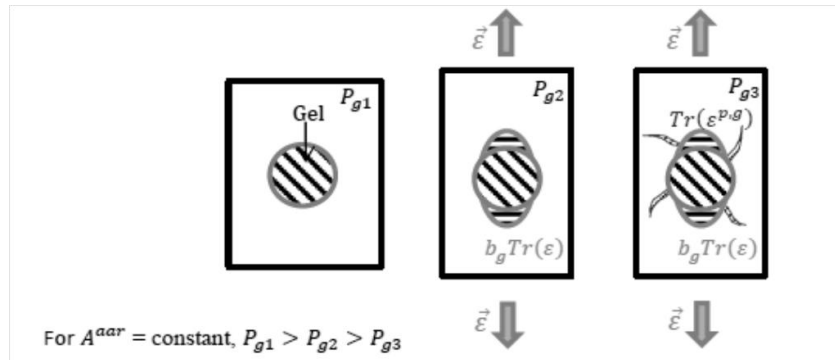


Figure 2 : Effect of strain on gel pressure

The concrete behaviour is modelled in the poro-mechanical framework. The model contains a damage model [2], and a creep model which considers a realistic interaction between AAR and structural behaviour. The creep model (Burger chain) is explained in Grimal and al [3] and by recent improvements in [9]. Concrete shrinkage during the same period can also be taken into account as illustrated in Figure 1.

The non-linear mechanical behaviour is described by using an anisotropic plastic criterion. Damage depends on plastic strains. In order to calculate plastic strains, there are two criteria groups: one to manage shear cracking (Drucker-Prager criteria) which is isotropic, and one to operate traction behaviour (Rankine criteria) which is orthotropic. The Rankine criteria distinguish between structural macro-cracks, reclosing macro-cracks and intra-porous pressure micro-cracks (AAR).

P_g is used to determinate micro-cracking due to AAR: criteria combines the stress state $\tilde{\sigma}_i$ and the gel pressure in each principal tensile stress direction.

LABORATORY TESTING CAMPAIGN

The walls used for the laboratory tests are 1.8 m x 1.44 m x 0.55 m and are reinforced by steel bars (Figure 3). 5 different walls are constructed with the same geometry: 3 with AAR concrete and 2 with regular concrete. They are tested at different aging times simultaneously under axial load and cyclic lateral load: Regular wall A at 240 days, regular wall B at 980 days, ASR wall A1 at 260 days, ASR wall B1 at 610 days, ASR wall B2 at 980 days. The aging is accelerated by storing the walls in a chamber maintained at 50°C and a relative humidity greater than 95%. The axial load is 800kN. The lateral load is cyclic, driven by displacements from 0 to 8.2 mm.

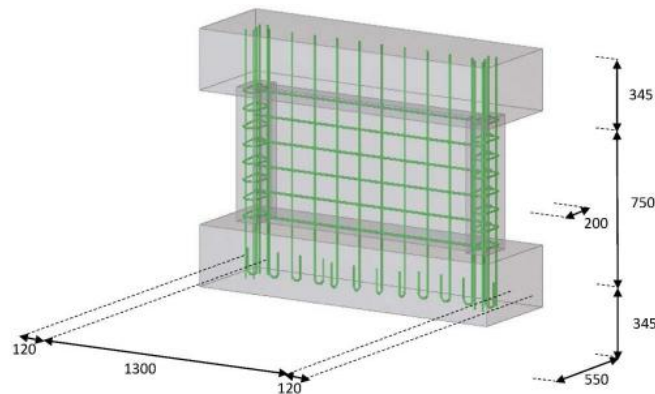


Figure 3 : Shear wall geometry



Figure 4 : Test Set Up

NUMERICAL MODEL

The concrete wall is meshed in 3D with hexadominant elements: 5870 elements, element size is around 30 mm. The steel reinforcements are meshed with 1D elements: 2390 elements.

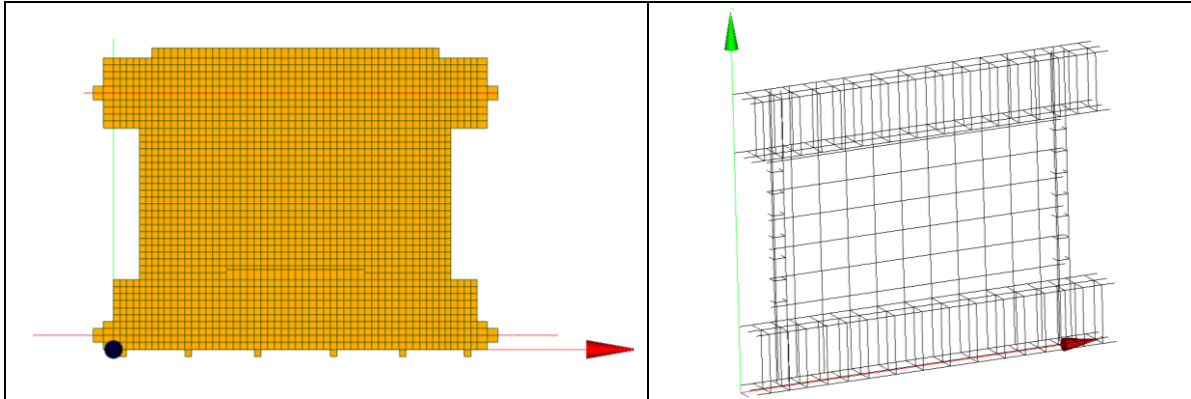


Figure 5 : Concrete mesh and reinforcement bars

As shown by the Figure 6, a special attention has been given to the modeling of the boundary conditions.

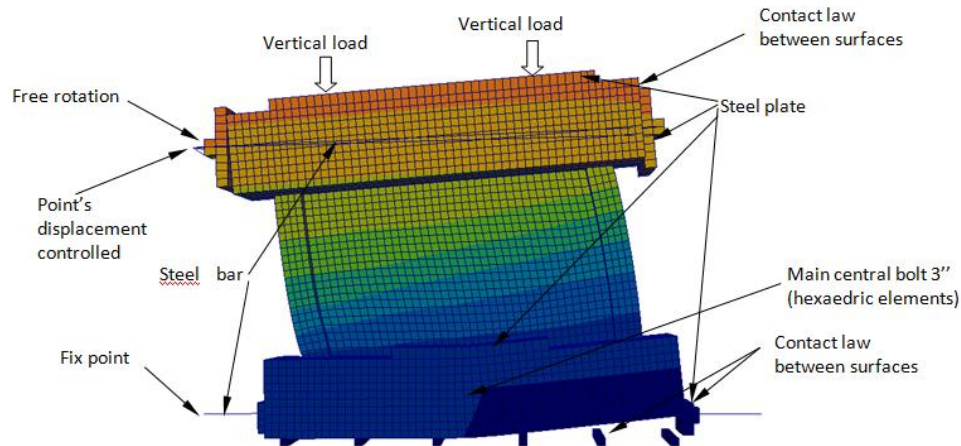


Figure 6 : Boundary conditions

RESULTS FOR THE REGULAR WALL

The plot of lateral load versus displacement given by the simulation is similar to the experimental results (Figure 7). The maximum lateral load that the wall can support is very well predicted by the simulation:

Experimental: $F_{max}=1180$ kN

Code_Aster: $F_{max}=1200$ kN

The model behavior is stiffer for the lower displacements (less than 5 mm) than in reality. The maximum applied load is reached for the model at about a 3 mm applied displacement instead of 5 mm. This could be explained by the fact that the model doesn't consider any sliding between concrete and reinforcement bars.

The tensile cracks start near the head of the central bolt or the bottom corner and have a diagonal propagation in the wall up to its top corner. Shear damages are also predicted by the simulation at the base of the wall. The simulated cracking pattern is coherent with the photos taken during the experimental campaign (Figure 7).

The simulation manages to reproduce the loading cycles with cracking opening, reclosure and failure.

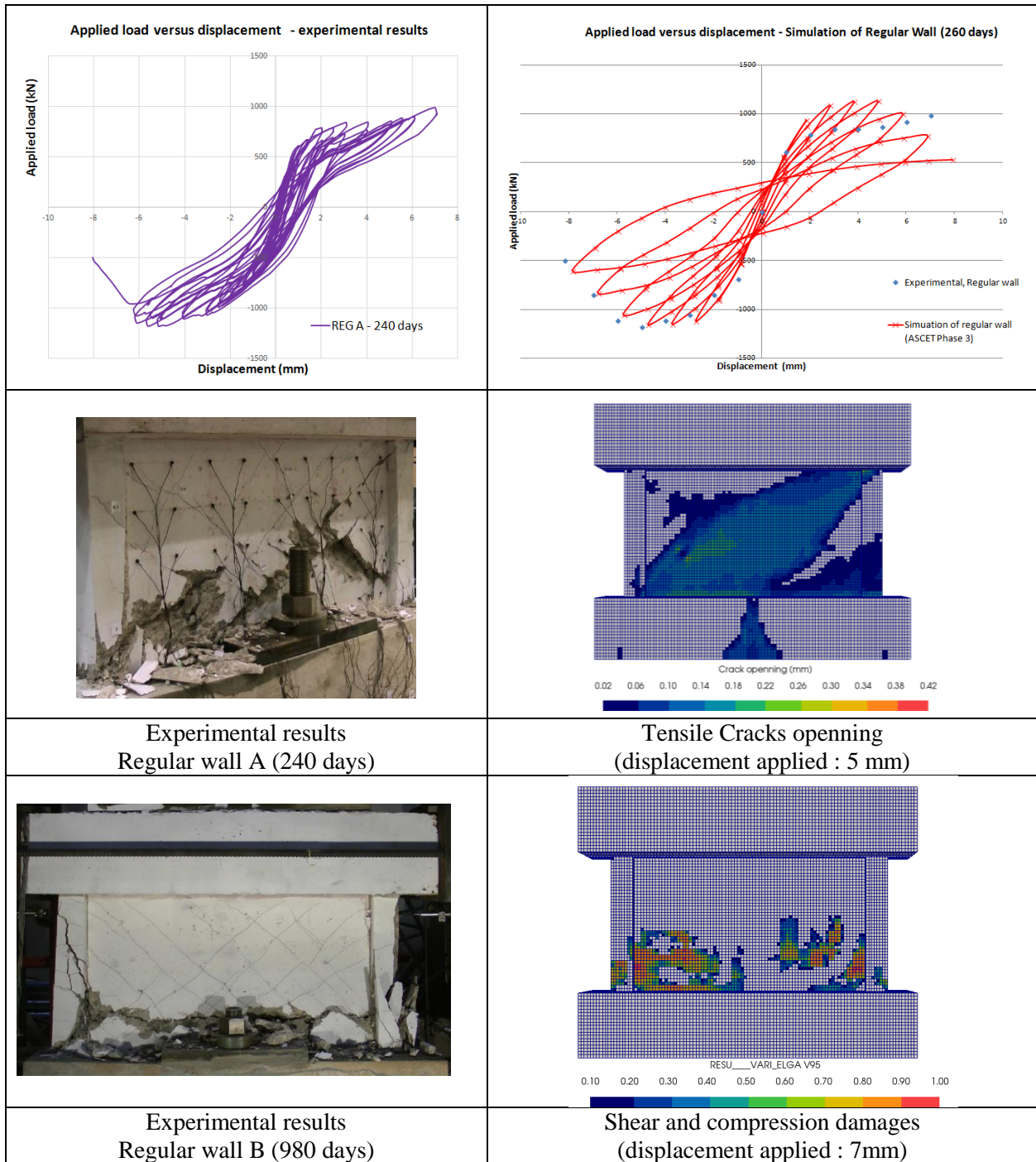


Figure 7 : Experimental (left column) and simulation results (right column) for regular walls

PRESTRESS IN THE ASR WALLS

The AAR parameters have been calibrated thanks to free expansion prisms. As shown by the Figure 8, the simulated free expansion curve fits well with the experimental results.

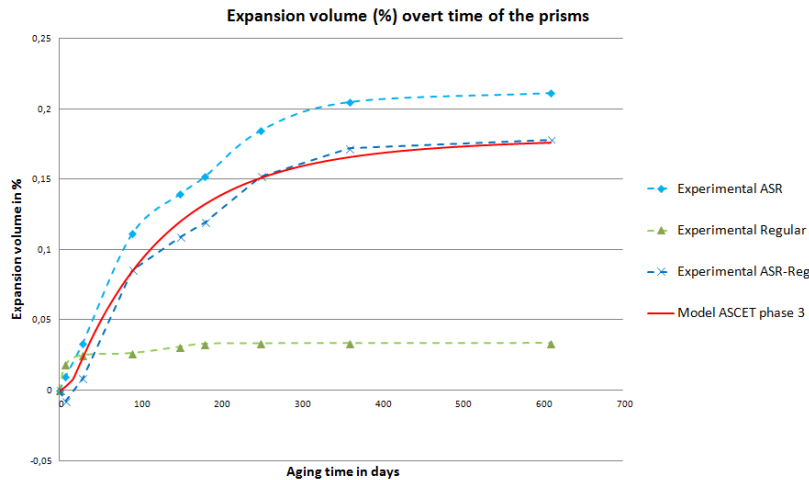


Figure 8 : Free expansion prisms (experimental and simulated)

Due to the reinforcements and the AAR, the wall concrete is prestressed. The main part of the wall at 260 days is prestressed at 1.8 to 1.9 MPa. At 980 days, the main part of the wall is prestressed at 2.3 to 2.9 MPa.

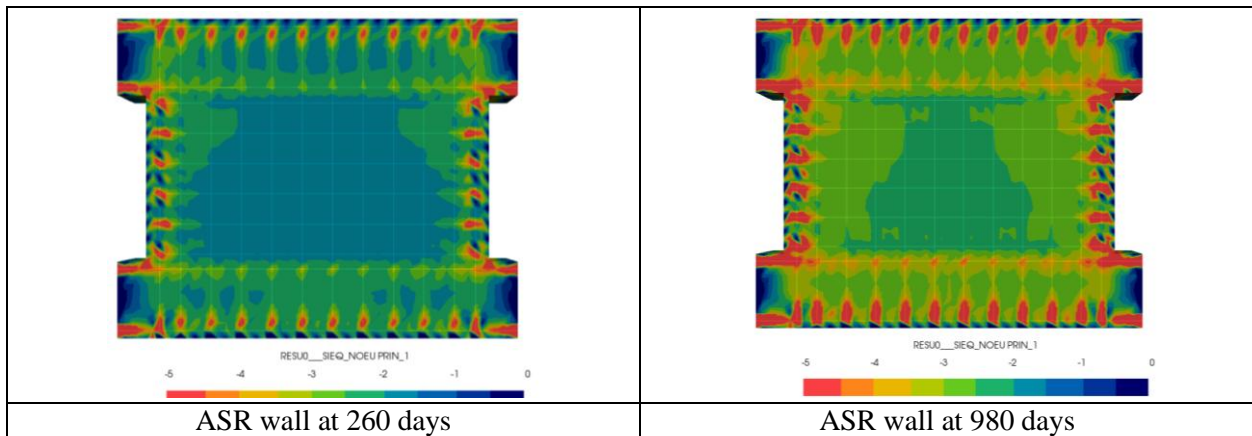


Figure 9 : Minimum principal stresses (compressions in MPa) in ASR walls

RESULTS FOR THE ASR WALL A1 AT 260 DAYS

The simulation plot of lateral load versus displacement fits well with the experimental results. The maximum load given by Code_Aster model is 1350 kN (1354.5 kN for the experimental test) and the failure of the model starts at 6 mm. The experimental failure of the wall can be seen during the second cycle at 6 mm.

The model reproduces well the fact that the wall with AAR has a higher resistance (higher maximum load applied). The confinement of the wall due to the beams, the presence of reinforcement bars and the swelling of the concrete due to AAR lead to the prestress of the wall and strengthen it, despite the degradation of concrete properties due to AAR.

In the same way as for the regular wall, cracks start from the bottom corner of the wall or at the central screw and propagate diagonally. This is coherent with the photo taken of the cracking pattern. The model indicates also shear damages at the bottom part of the wall.

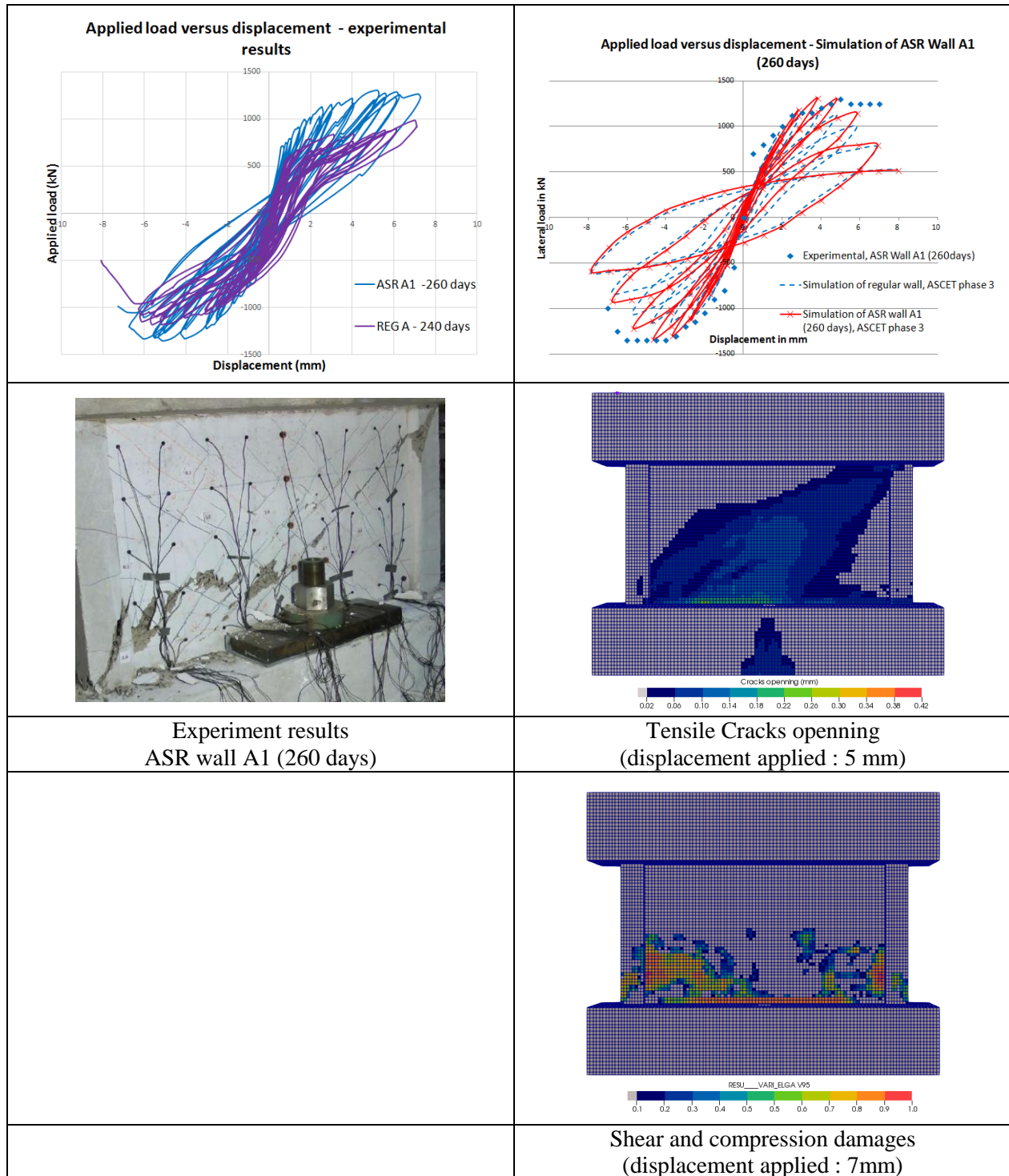


Figure 10 : Experimental (left column) and simulation results (right column) for ASR wall A1 (260 days)

RESULTS FOR THE ASR WALL B2 AT 980 DAYS

The results after 980 days of accelerated aging are similar to the results after 260 days. The maximum lateral load is 1390 kN. The experimental result is 1157 kN. But it has to be reminded that the ASR wall A1 (260 days) was able to resist to a maximum load of 1354.5 kN.

The behaviour of the experimental walls at 610 days and 980 days with alkali aggregate reaction experiences with time a significant loss of ductility and energy absorption. The hysteretic loops became very narrow. The simulation has not reproduced this loss of ductility. The simulation shows a similar cracking pattern to the simulation results at 260 days, showing a diagonal propagation. This is coherent with the experimental failure mechanism.

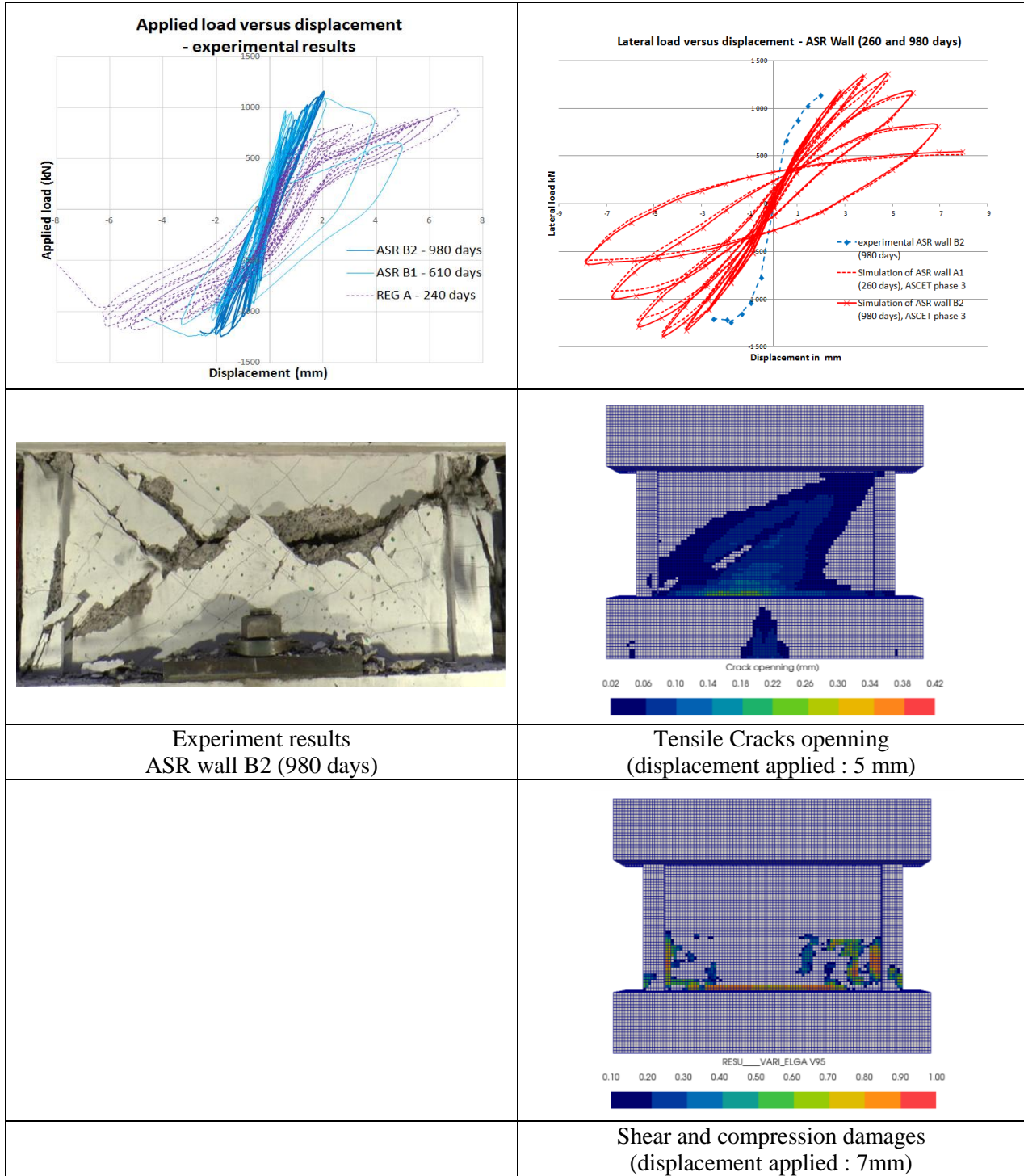


Figure 11 : Experimental (left column) and simulation results (right column) for wall B2 (at 980 days)

CONCLUSION

The RGI model integrated in Code_Aster has been able to reproduce the Alkali Aggregate Reaction in a shear wall and the cycling loading tests. Cracking pattern and load versus displacement curve have been compared to the experimental results. The simulation gives a good prediction of the wall behaviour for the regular walls and the AAR wall after 260 days of accelerated aging. The simulation reproduces the gain of resistance of the AAR wall due to the prestress of the concrete despite the degradation of mechanical properties due to AAR. After 610 days and 980 days of accelerated aging, the experimental results show a loss of ductility of the walls. The simulation has not reproduced this behaviour. Nevertheless, the failure mechanism is well reproduced and the maximum load applied is slightly overestimated.

REFERENCES

- [1] Biot M.A. (1972), « Theory of finite deformation of porous solids », *Indiana Univ. Math. J.* 21, 579–620.
- [2] Coussy O (1995), « Mechanics of Porous Continua », J. Wiley & Sons, Chichester, UK.
- [3] Grimal E., Sellier A., Le Pape Y., Bourdarot E. (2008), « Creep, shrinkage, and anisotropic damage in alkali-aggregate reaction swelling mechanism-Part I: A constitutive model », *ACI Materials Journal*, 105(3).
- [4] Kim T., Olek J. (2014), « Chemical Sequence and Kinetics of Alkali-Silica Reaction Part II. A Thermodynamic Model », *Journal of the American Ceramic Society*, 97(7), pp. 2204-2212.
- [5] Morenon P., Multon S., Sellier A., Grimal E., Hamon F., Bourdarot E. (2016), « Impact of multi-axial stresses on ASR expansion », *15th ICAAR*, Sao Paulo, 180.
- [6] Perruchot A., Massard P., Lombardi J. (2003), « Composition et volume molaire apparent », *Comptes Rendus Geoscience*, 335(13), 951-958.
- [7] Poyet S. (2003), « Etude de la dégradation des ouvrages en béton atteints par la réaction alcali silice : Approche expérimentale et modélisation numérique multi-échelles des dégradations dans un environnement hydro-chemo-mécanique variable », thèse de doctorat de l'université de Marne la Vallée.
- [8] Sellier A., Casaux-Ginestet G., Buffo-Lacarrière L., Bourbon X. (2013), « Orthotropic damage coupled with localized crack reclosure processing. Part I: Constitutive laws », *Engineering Fracture Mechanics*, 97, 148-167.
- [9] Sellier A., Multon S., Buffo-Lacarrière L., Vidal T., Bourbon X., Camps G. (2016), « Concrete creep modelling for structural applications: non-linearity, multi-axiality, hydration, temperature and drying effects », *Cement and Concrete Research*, Vol. 79, pp. 301–315.